Mineralogical Magazine, June 2006, Vol. 70(3), pp. 265–280

The missing sulphur in mattheddleite, sulphur analysis of sulphates, and paragenetic relations at Leadhills, Scotland

E. J. Essene[1,*], C. E. Henderson[1] and A. Livingstone[2]

[1] Department of Geological Sciences, University of Michigan, Ann Arbor MI 48109-1063, USA
[2] 6, St. Ronan's Terrace, Innerleithen, Peeblesshire EH44 6RB, UK

ABSTRACT

Published electron microprobe analyses of mattheddleite, a lead sulpho-silicate apatite from Leadhills, Scotland, have 9–13% IV site deficiencies. However, galena was used as a standard for S, which suggested that low S resulted from a shift in the S-$K\alpha$ peak. Wavelength scans with a PET crystal show that the S-$K\alpha$ peak is shifted down by 0.0026 Å for sulphates relative to sulphides. Quantitative analyses show a ~30% increase of S in mattheddleite using a celestite standard, which fills the IV site, but with Si > S, on average $Pb_5S_{1.2}Si_{1.8}O_{11.7}Cl_{0.6}(OH)_{0.4}$. Direct analysis of oxygen with the electron microprobe implies that the charge imbalance engendered from the inequality of Si and S is compensated with substitution of a vacancy (□), as in $Pb_5S_{1.2}Si_{1.8}[O_{11.7}\square_{0.3}][Cl_{0.6}(OH)_{0.4}]$ or $Pb_5S_{1.2}Si_{1.8}[O_{11.7}(Cl,OH)_{0.3}][Cl,OH)_{0.7}\square_{0.3}]$. Calculation of OH as 1−Cl suggests the presence of both OH- and Cl-dominant mattheddleite at Leadhills, but direct analysis of H is needed to confirm the dominance of OH in the channel site. Wavelength-dispersive analyses of S in apatite and other sulphates must be undertaken with sulphate standards: use of sulphide standards yields a negative error on the order of 10–20% in the resultant S concentration. Reactions of mattheddleite with other Pb minerals at Leadhills show that their stability depends on fluid composition as well as pressure and temperature. An X-ray map of Cl shows complex zoning between Cl-poor and Cl-rich mattheddleite, recording rapid changes in the fluid chemistry during late-stage hydrothermal processes at Leadhills.

Keywords: mattheddleite, sulphate, apatite, wavelength shift, Cl migration, Leadhills, phase equilibria.

Introduction

Sulphatoan apatite is known to occur as a result of charge-compensated substitutions that allow S^{6+} to substitute for P^{5+} in the IV site. Exchange involving sulphate in the apatite group includes (1) $2P^{5+} = Si^{4+}S^{6+}$, which points towards ellestadite, $Ca_5(SiO_4)_{1.5}(SO_4)_{1.5}(F,Cl,OH)$ (e.g. McConnell, 1937; Harada *et al.*, 1971) and mattheddleite, $Pb_5(SiO_4)_{1.5}(SO_4)_{1.5}(Cl,OH)$ (Steele *et al.*, 2000); and (2) $R^{2+}P^{5+} = Na^{+}S^{6+}$, which leads to cesanite, $Na_3Ca_2(SO_4)_3OH$ (Cavarretta *et al.*, 1981; Piotrowski *et al.*, 2002; Chakhmouradian and Medici, 2006) and caracolite, $Na_3Pb_2(SO_4)_3Cl$ (Seeliger and Berdesinski, 1956). An X-ray structure refinement by Hughes and Drexler (1991) on hydroxylellestadite revealed partial ordering of Si and S in different IV sites, which should also be evaluated for mattheddleite. Apatite with minor sulphate has been reported in oxidized granites (Peng *et al.*, 1997; Streck and Dilles, 1998; Barth and Dorais, 2000; Core *et al.*, 2006), carbonatites and alkaline igneous rocks (Liu and Comodi, 1993), and in hydrothermal veins (Shiga and Urashima, 1987). Apatite from most igneous and metamorphic rocks has approximately stoichiometric substitution on the VIII and IV sites, but electron microprobe analyses of mattheddleite yielded 8% (Livingstone *et al.*, 1987) and 13% (Steele *et al.*, 2000) deficiency on the IV site. In their refinement of the crystal structure of mattheddleite Steele *et al.* (2000) assumed full occupancy of the IV site with Si = S. They concluded that the absorption correction in the microprobe analysis

* E-mail: essene@umich.edu
DOI: 10.1180/0026461067030330

© *2006 The Mineralogical Society*

of S had a systematic error, and that the mattheddleite formula is $Pb_5(SiO_4)_{1.5}(SO_4)_{1.5}$ (Cl,OH). It is difficult to distinguish Si from S in an X-ray structure refinement, and that conclusion is in need of further tests.

Livingstone *et al.* (1987) and Steele *et al.* (2000) used galena as a standard for wavelength dispersive (WDS) analyses of mattheddleite with an electron microprobe. However, the peak position of the S-$K\alpha$ line is known to shift to lower wavelengths in sulphates relative to sulphides. Measurements of the peak shift on the electron microprobe using sulphate and sulphide standards was used nearly 40 y ago to identify the valence state of sulphur in the biotite group mineral anandite (Lovering and Widdowson, 1968*a,b*). The shift has also been used to determine whether sulphide or sulphate is substituted in silicate glass (Connolly and Haughton, 1972; Carroll and Rutherford, 1988; Wallace and Carmichael, 1994; Matthews *et al.*, 1999). It seemed likely, therefore, that the deficiency in the IV site of mattheddleite might be an artifact of the standards rather than representing a real IV deficiency or one related to errors in mass absorption coefficients.

Sample description

The minerals of the Leadhills district in Scotland have been described by Brown (1919), Temple (1956), Gillanders (1981) and Livingstone (2002). The Pb minerals in the system Pb-Si-C-O-S-H that have been reported at Leadhills include anglesite ($PbSO_4$), cerussite ($PbCO_3$), galena (PbS), hydrocerussite ($Pb_3(CO_3)_2(OH)_2$), lanarkite (Pb_2OSO_4), lead (Pb), minium (Pb_3O_4), plattnerite (PbO_2), scotlandite ($PbSO_3$), and the polymorphs of $Pb_4SO_4(CO_3)_2(OH)_2$ (leadhillite, macphersonite, susannite) (Temple, 1956; Abdul-Samad *et al.*, 1982; Livingstone and Sarp, 1984; Paar *et al.*, 1984*b*; Livingstone and Russell, 1985; Livingstone *et al.*, 1987; Livingstone, 2002). Other Pb minerals in this system include alamosite, $PbSiO_3$, and plumbotsumite, $Pb_5Si_4O_8(OH)_{10}$, which have been found at Tsumeb (Keller and Dunn, 1982). Brown (1919) suggested that some samples of minium might be the product of smelting at Leadhills, and it is possible that the occurrences of native lead there have a similar origin. Livingstone *et al.* (1987) characterized the new mineral mattheddleite from a secondary vein at Leadhills associated with quartz-caledonite-cerussite-leadhillite-susannite-macphersonite and lanarkite-cerussite-hydrocerussite-leadhillite-caledonite.

A mattheddleite sample from Leadhills, Scotland, was used to evaluate the wavelength shift in its S-$K\alpha$ peak and compare analyses using sulphide *vs*. sulphate standards. It is sample NMS G 1878.49.488.2 from the National Museums of Scotland and is labelled as 'mattheddleite with leadhillite and susannite from Leadhills, Lanarkshire', the same sample as studied by Steele *et al.* (2000). The mattheddleite sample consists of small aggregates of transparent crystals. It was mounted in epoxy, polished and examined with backscattered electron (BSE) imaging on a CAMECA SX-100 electron microprobe. The BSE image shows central areas with blades with a higher average atomic number (Z) intergrown with large euhedral crystals with lower Z, all surrounded by equant to elongate crystals with intermediate contrast (Fig. 1). Energy dispersive spectroscopy (EDS) shows that the latter area has Pb±S, Si and Cl, which is consistent with mattheddleite. The two intergrown phases in the interior of the crystal aggregate are both rich in Pb±S but lack Si and Cl. Anglesite,

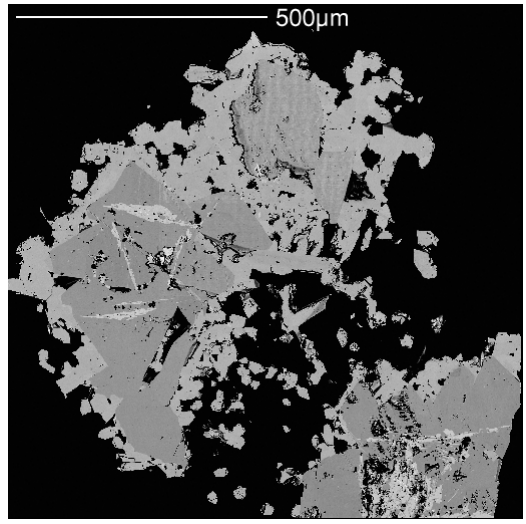

FIG. 1. BSE image of a lower Z (darker contrast) Pb sulphate (leadhillite and/or susannite) with high Z (bright contrast) blades (hydrocerussite) and rims of intermediate Z phase (mattheddleite). The dark areas were voids (now plastic). The vertical bands in the leadhillite are the result of electron beam damage. Image collected at 15 kV, 30 nA, a point beam, and a 2 µm step per pixel, 200 ms dwell time per pixel, for the 1024 × 1024 µm scan, total time 14 h.

cerussite, galena, hydrocerussite, lanarkite, scotlandite and the leadhillite polymorphs are difficult to distinguish with routine EDS observations on a carbon-coated sample as a result of severe overlap of S-*K*α and Pb-*M*α peaks, and the potential contribution of the carbon coat to C-*K*α. The average atomic number Z (in parentheses) of each end-member mineral was calculated from the ideal formulae as follows: anglesite (59.4), scotlandite (62.3), the leadhillite polymorphs (65.0), cerussite (65.3), lanarkite (66.7), hydrocerussite (67.2), shannonite (70.5) and galena (73.2). The average Z for Cl-mattheddleite (65.3) and OH-mattheddleite (65.7) was calculated using an idealized formula with Si=S, comparable to an average Z of 65.5 calculated directly from analytical data in this paper for the real mattheddleite. It is evident that most of the Pb minerals have a larger Z than mattheddleite. The low Z phase inside the mattheddleite aggregates is probably leadhillite, although the presence of susannite or macphersonite cannot be excluded.

Slow BSE scans revealed subtle contrast in the mattheddleite (Fig. 1), and X-ray mapping of the Cl was therefore undertaken. Images that were first collected over 20 min showed Cl zoning but were noisy because of the relatively low count rates for Cl. Additional slower scans were obtained including a 14 h scan (Fig. 2). They show remarkable oscillatory zoning in the Cl content of the mattheddleite that is only poorly resolved even in the BSE image obtained at lower magnification (Fig. 1). A spectacular SEM image of a variably resorbed mattheddleite specimen from Caldbeck Fells was shown by Cooper and Stanley (1990). Several zones of high, low and

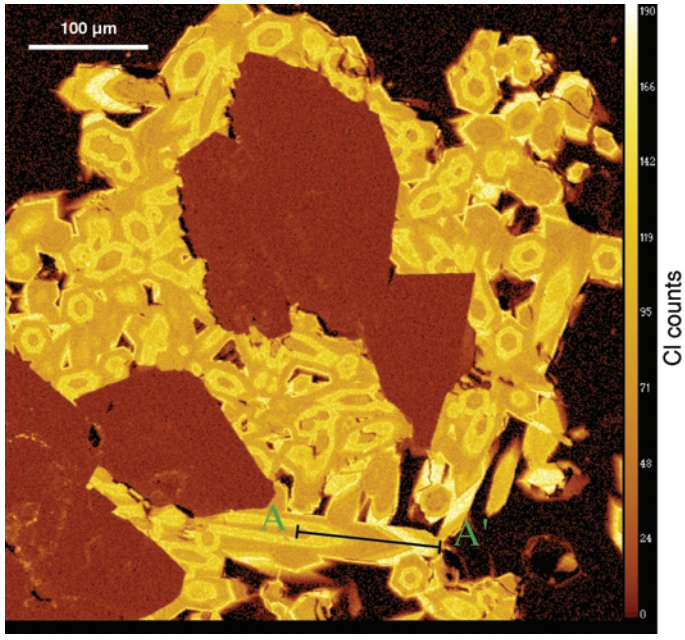

FIG. 2. False colour X-ray map of Cl distribution showing a leopard-skin pattern in zoned mattheddleite. The Cl map reveals at least seven growth zones with different Cl, best seen in the labelled elongate grain near the bottom of the image (traverse shown in Fig. 3). Scan conducted at 15 kV, 30 nA, a point beam, 1 µm step per pixel, 200 ms dwell time per pixel, for the 512 × 512 µm scan, and total time 14 h. The yellowish-white areas (stage 6) have the highest Cl (~2.5 wt.% Cl), and the golden brown areas have the lowest Cl (~1 wt.% Cl). Using the lighter areas as a guide allows one to identify the timing of growth of the mattheddleite aggregates. In hexagonal cross-sections, one can see the white-yellow near a few margins, but stage 2 growth (lighter yellow, itself delicately zoned in Cl, cf. dip in peak shown in Fig. 3) is more commonly developed in the cross-sections. The large crystals (orange-brown euhedra) overgrown by mattheddleite are a leadhillite polymorph with blades of hydrocerussite (cf. Fig. 1), and marginal, deep brown areas are cavities filled by epoxy. The leadhillite and hydrocerussite have a higher background reading for Cl than the epoxy, which produces minor apparent Cl in the scan, which is uncorrected for Cl background. Cl analyses along the line A–A′ are shown in Fig. 3.

medium Cl growth are best resolved in long cross-sections. The large crystal with the line near the bottom of Fig. 2 was selected for a detailed traverse. From the core outward, zones 1 and 4 are lowest in Cl (dark brown areas), and zone 6 is highest (yellowish-white areas). One elongate grain in the image was selected for a detailed analytical traverse; the result shows that the Cl has two peaks of growth with declining values between the peaks (Fig. 3). The initially separate, euhedral crystals were welded together into a leopard-skin mass primarily during growth of zone 4. Cathodoluminescence images were collected on the same area as Fig. 2 but revealed little contrast.

Analytical procedures

Analytical conditions that were employed are summarized in Table 1. Natural alamosite, $PbSiO_3$ (Boucher and Peacor, 1968) has been demonstrated by electron microprobe analysis to have no observable solid solutions, and it was used for the analysis of Pb, Si and O. For comparison, a galena standard was used for Pb and S, and a CAMECA routine that shifts the wavelength position between standards and unknowns was also employed (Table 2). Wavelength scans over S-*K*α were obtained on mattheddleite, anhydrite, celestite, pyrite, troilite and galena. The scans were centred around the peak on four different PET crystals on the SX-100 electron microprobe at the University of Michigan (Fig. 4). The CAMECA peaking routine yields a shift of 0.0026 Å (30 in 10,000 Sinθ units) in the peak positions between the sulphides and the sulphates. A similar shift is the basis for distinguishing sulphate *vs.* sulphide species in basaltic glass (e.g. Carroll and Rutherford, 1988). Peaking the S-*K*α peak on a sulphide standard with default CAMECA procedures places the spectrometer on the shoulder of the S-*K*α peak for sulphates, thus giving low peak S values for sulphate unknowns. Analysing a peak on its shoulder means that the result is sensitive to the exact shape and location of the peak, which depends on the diameter of the Rowland circle, the detector slit size, the spectrometer crystal and its size, each of which may vary from machine to machine. Thus, one cannot anticipate a fixed correction to the low S that is caused by the wavelength shift in different laboratories, and it should be calibrated in each facility.

Wavelength scans were also conducted across the Pb-*M*α and S-*K*α peaks in order to select background measurement positions for Pb and S that avoid striking the tails of the other peaks (Fig. 5). Careless placement of the low-wavelength background position for Pb and the high-wavelength background setting for S may lead to reduced Pb or S levels in mattheddleite due to an anomalously raised background for Pb or S. Wavelength scans conducted across Pb-*M*γ and Cl-*K*α on mattheddleite showed that no background interference was encountered during quantitative analysis of its Cl.

Trace and minor elements were analysed separately at higher current and over a longer period to improve the detection limits (Table 1). The elements F, Ca, Mn, V, As, Sr, Y, Ba, La, Ce, Pr, Nd, Sm, Gd and Th were analysed both in mattheddleite and the alamosite standard. To

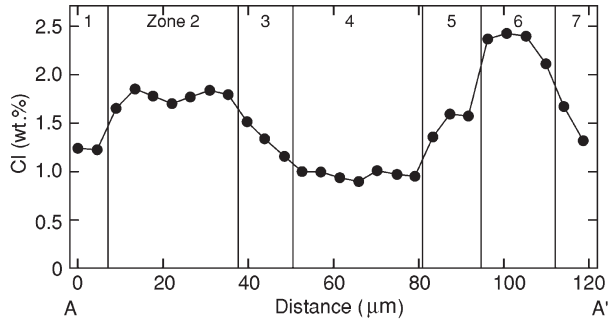

FIG. 3. Traverse of wt.% Cl for the elongate grain (marked as line A–A′ in Fig. 2) showing variation in Cl along the length of the mattheddleite crystal. The second zone near the core of the grain is to the right and the rim is to the left. The very narrow zone of low Cl in the core of the elongate crystal was unintentionally excluded from the scan. The value of 1.0 wt.% Cl for stage 3 corresponds to 0.37 Cl p.f.u. and 2.5 wt.% Cl for stage 6 is ~0.93 Cl p.f.u. Every third analysis from this traverse is in Table 3.

TABLE 1. Analytical conditions for analysis of mattheddleite[1].

Element line	Crystal[4]	Standards	Background λ shift[2]	DL (ppm)[3]
F-*K*α	PC1	Henry Mtns. fluor-topaz	±2000	330
O-*K*α	LPC0	Peacor alamosite	+4000, −3000	1100
Na-*K*α	LTAP	Tiburon albite	±500	260
Si-*K*α	TAP	alamosite, wollastonite	±500	320
P-*K*α	LPET	synthetic alforsite	±500	580
S-*K*α	LTAP	Maybee celestite	+540, −1870	360
Cl-*K*α	PET	synthetic alforsite	±500	440
Ca-*K*α	PET	ANU wollastonite	±500	360
Mn-*K*α	LLIF	Broken Hill rhodonite	±500	270
V-*K*α	LLIF	synthetic V_2O_5	±900	230
As-*L*α	LTAP	natural olivenite	±600	250
Sr-*L*α	LPET	Maybee celestite	±500	700
Y-*L*α	PET	syn. Y-Al garnet (YAG)	−1600, slope 0.81	520
Ba-*L*α	LLIF	synthetic alforsite	±500	1100
La-*L*α	LLIF	synthetic $LaPO_4$	±500	980
Ce-*L*α	LLIF	synthetic $CePO_4$	±500	970
Pr-*L*β	LLIF	synthetic $PrPO_4$	−520, slope 1	2260
Nd-*L*α	LLIF	synthetic $NdPO_4$	+1800, −1930	960
Sm-*L*β	LLIF	synthetic $SmPO_4$	530, −512	1340
Gd-*L*β	LLIF	synthetic $GdPO_4$	520, −420	1420
Pb-*L*α	PET	Peacor alamosite, galena	+1500, −900	1330
Th-*M*α	PET	synthetic $ThSiO_4$	+800, −1300	1250

[1] analyses at 15 kV, 10 nA, 5 μm beam, 30 s for peak, 30 s for background(s)
[2] units 10,000*Sinθ
[3] DL = detection limit of individual analysis
[4] L, in front of PC0, TAP, PET, LIF means large spectrometer crystal

minimize interferences, Lβ lines were used for Pr, Sm and Gd, and Mβ was chosen for Th (Table 1). None of the above elements was found at a level exceeding its detection limit. The detection limit of the heavy elements (Ba, *REE*, Th) is in the range 900−1400 ppm, not optimal for their

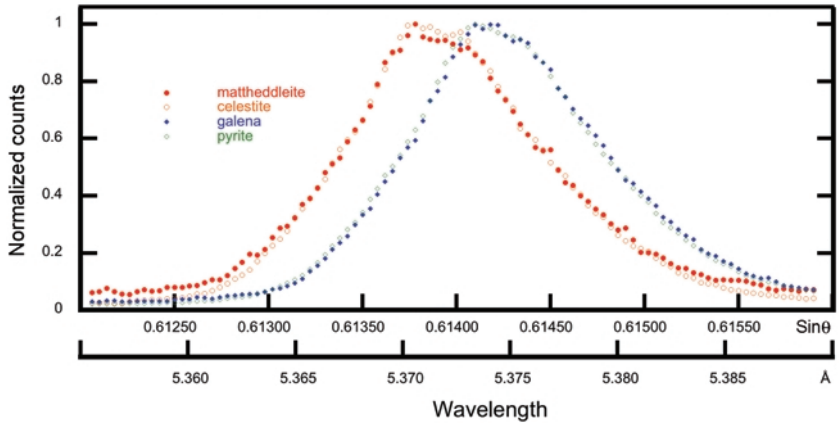

FIG. 4. Wavelength scans across the S-*K*α peaks of mattheddleite, anhydrite, celestite, pyrite and galena using a PET crystal ($2d$ = 8.75 Å). The counts are normalized to unity for the highest point on each scan to facilitate comparisons among the different phases. The peak positions of the sulphates are at ~5.372 Å and the sulphides at 5.374 Å. The S-*K*α peak for troilite (not shown) is located at the same position as that for galena and pyrite.

TABLE 2. Mattheddleite analyses with different procedures[1].

Standard	Celestite	Galena	Galena shifted[2]
Wt.% oxide			
SO_3	7.20	5.57	6.90
P_2O_5	n.d.[3]	n.d.	n.d.
SiO_2	7.84	7.88	7.90
PbO	82.89	82.96	82.83
Cl	1.45	1.36	1.39
H_2O[4]	0.31	0.32	0.32
Cl=O	−0.32	−0.25	−0.26
Sum[5]	99.27	97.84	99.08
Atoms[6]			
S	1.21	0.94	1.16
P	0.00	0.00	0.00
Si	1.76	1.76	1.77
Pb	5.00	5.00	5.00
O	11.65	10.85	11.53
Cl	0.55	0.52	0.53
OH[7]	0.45	0.48	0.47
IV site	2.97	2.70	2.93

[1] average analysis of the same 9 points as in Table 2
[2] shift in peak position corrected with a Cameca routine
[3] not detected
[4] back-calculated
[5] incl. −Cl=O
[6] normalized to Pb = 5
[7] 1−Cl

analysis. Those elements are best analysed on an electron microprobe at higher voltage and current, but under such conditions mattheddleite is rapidly damaged, such that the result is compromised. If one wishes to improve the analytical results for these trace elements, another analytical technique such as inductively couple plasma-mass spectroscopy should be employed.

The possibility of Cl migration during electron microbeam analysis, as was reported in chlorapatite (Stormer *et al.*, 1993), is also in need of evaluation before undertaking quantitative analysis of apatite group minerals. To evaluate migration of Cl, time tests were undertaken with (1) a point beam at 15 kV and 25 nA (the analytical conditions of Steele *et al.*, 2000), (2) a point beam at 15 kV and 10 nA, and (3) a 5 μm wide beam at 15 kV and 10 nA. The results of (1) and (2) show a gradual Cl increase in the apatite with time, whereas (3) shows no change in Cl within the precision of the method (Fig. 6). The effect on the Cl analyses of Steele *et al.* (2000) depends on the Cl counting time and whether Cl was the first element analysed on a given spectrometer (which is likely in this case). The Cl content as measured by Steele *et al.* (2000) would have risen by ~1.4 % of the amount present (OAP) over 30 s and by 2.8% OAP over 60 s, with the average Cl increasing by half that during the total counting time, or only 0.015−0.027 wt.% at 30−60 s of analysis time, an insignificant increment. The effect of orientation described by Stormer *et al.* (1993) was also evaluated by time tests with a point beam on Cl-rich areas from a hexagonal cross section *vs*. a long section of apatite, but the results were similar until after 8 min, after which the measured Cl in the cross-section was lost more rapidly. The amount of Cl increase at a given voltage, current and beam size depends on the total electron

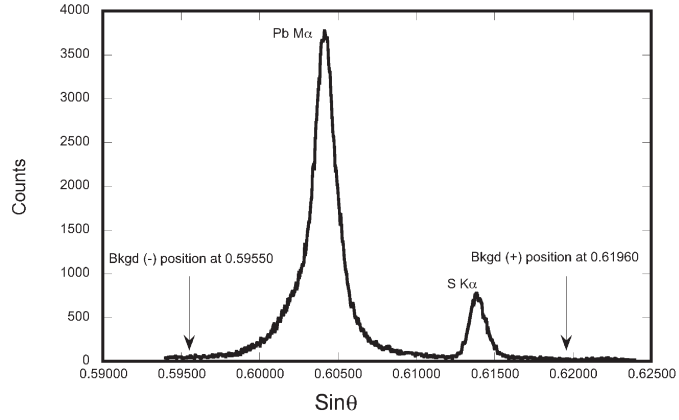

FIG. 5. Wavelength scan across the Pb-*M*α and S-*K*α peaks showing the placement of the locations of background positions for both Pb and S.

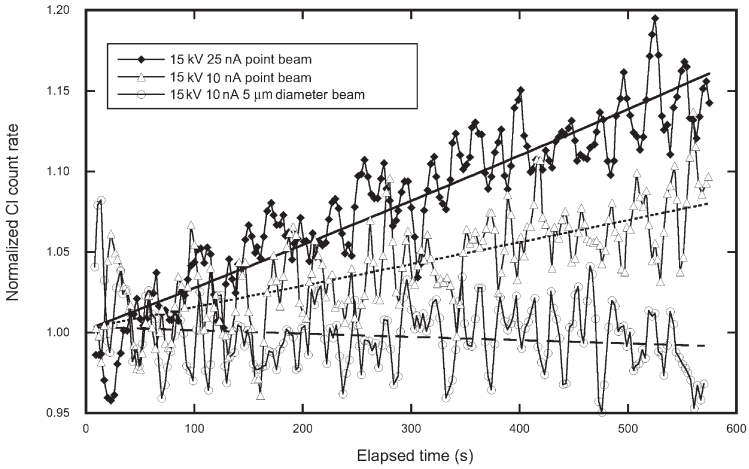

FIG. 6. Time tests of apparent Cl levels (◆) with a point beam at 15 kV and 25 nA; (△) with a point beam at 15 kV and 10 nA; and (○) with a 5 μm wide beam at 15 kV and 10 nA.

exposure time before which the Cl analysis is completed. Such tests are essential before undertaking quantitative measurements of halogens on apatite, but mattheddleite does not appear to be perturbed for analysis at reasonable times and currents, even with a point beam.

Oxygen was analysed directly on mattheddleite to evaluate the possibility of an anion deficiency resulting from the inequality of Si and S in the formula. Natural alamosite (Boucher and Peacor, 1968) was selected as a standard after preliminary calculations of ZAF factors for O between mattheddleite and alamosite showed only minor corrections. Mineral formulae in this study were calculated with cation-based normalization procedures (e.g. Afifi and Essene, 1988; Essene, 1989). The mattheddleite analyses were normalized to 5 Pb atoms because the numbers of anions were not measured directly, and the occupancy of the IV site (S+Si) is under evaluation in this contribution. The average O in the mattheddleite sample is 12.1 per formula unit (p.f.u.), and subtracting 0.4 p.f.u. OH assuming it is equal to 1−Cl leaves 11.7 (p.f.u.) for the framework O (Table 3).

Quantitative analyses of mattheddleite were obtained using both galena and celestite as standards for S. The OH was calculated as 1−Cl and the equivalent wt.% H_2O was back-calculated from the molar OH (Tables 2−5). For analysis of the host hydrocerussite and leadhillite, the wt.% CO_2 was initially calculated as the difference from 100% in order to provide an adequate matrix for the ZAF corrections. The Pb and S levels in the analyses indicate that the low-Z phase in the host is a leadhillite polymorph and the high-Z blades are hydrocerussite. The CO_3 and OH were assumed to be stoichiometric in these two phases and the wt.% H_2O and CO_2 in the analyses was back-calculated (Table 5). The high totals in hydrocerussite are attributed to partial degassing of H_2O and/or CO_2 that produced an increased wt.% PbO during the analysis. Its low apparent S and Si may also reflect fluorescence of S and Si by Pb X-rays interacting with the surrounding leadhillite.

Analytical results

The wavelength scans in the position of the S-$K\alpha$ peak showed a systematic shift of the sulphides *vs*. the sulphates including mattheddleite (Fig. 4). Electron microprobe analysis of mattheddleite using sulphide standards will yield low S because the peak position for the sulphides is located on the shoulder of the S peak for mattheddleite. That was confirmed by direct analysis of the mattheddleite using celestite as a standard for S (Table 4) compared to galena (Table 2). The apparent S level of mattheddleite analysed with a celestite standard is ~30% higher than that analysed with a galena standard. This observation shows why electron microprobe analyses in Livingstone *et al.* (1987) and Steele *et al.* (2000) produce deficiencies on the IV site of mattheddleite. The peak shift routine using a galena standard improved the mattheddleite analyses, although the result for S is still not the same as that using a celestite standard

TABLE 3. Analyses along a traverse of mattheddleite including direct measurement of oxygen[1].

Wt. %	2	5	8	11	14	17	20	23	26	29	32	35	38	ave.[2]	s.d.[2]
S	2.81	2.76	2.83	2.80	2.82	2.83	3.07	2.98	3.01	2.96	2.98	3.03	3.03	2.90	0.12
P[3]	0.03	0.01	0.00	0.00	−0.02	0.00	0.02	0.01	0.02	−0.03	−0.03	0.00	0.00	0.00	–
Si	3.80	3.61	3.76	3.75	3.83	3.75	3.54	3.60	3.62	3.71	3.61	3.68	3.53	3.65	0.10
Pb	76.04	76.15	77.21	77.60	76.54	75.97	77.07	76.65	76.76	76.59	76.51	77.07	76.91	76.67	0.44
O	14.73	14.69	14.61	14.47	14.53	14.68	14.15	14.13	14.13	14.50	14.29	14.01	14.09	14.58	0.24
Cl	1.67	2.45	1.60	0.98	0.94	1.16	1.80	1.71	1.67	1.35	1.49	1.65	1.86	1.57	0.10
H[4]		0.01	0.07	0.12	0.12	0.10	0.05	0.06	0.06	0.09	0.08	0.07	0.05	0.07	0.01
Cl=O	−0.37	−0.61	−0.54	−0.35	−0.22	−0.21	−0.26	−0.40	−0.38	−0.37	−0.30	−0.33	−0.36	−0.34	–
Sum	98.71	99.68	100.08	99.72	98.76	98.48	99.69	99.15	99.25	99.11	98.88	99.50	99.46	99.37	0.45
Atoms[5]															
S	1.20	1.17	1.19	1.17	1.19	1.20	1.29	1.26	1.27	1.25	1.26	1.27	1.27	1.22	0.05
P[3]	−0.01	0.00	0.00	0.00	0.00	0.00	0.00	0.00	0.00	−0.01	−0.01	0.00	0.00	0.00	–
Si	1.84	1.75	1.80	1.79	1.85	1.82	1.70	1.73	1.74	1.79	1.74	1.76	1.69	1.77	0.05
Pb	5.00	5.00	5.00	5.00	5.00	5.00	5.00	5.00	5.00	5.00	5.00	5.00	5.00	5.00	0.00
O	12.54	12.50	12.26	12.08	12.30	12.51	11.89	11.94	11.93	12.27	12.10	11.78	11.87	12.12	0.24
Cl	0.64	0.94	0.60	0.37	0.36	0.45	0.68	0.65	0.63	0.51	0.57	0.63	0.71	0.59	0.15
OH[6]	0.36	0.06	0.40	0.63	0.64	0.55	0.32	0.35	0.37	0.49	0.43	0.37	0.29	0.41	0.15
IV site	3.04	2.93	2.98	2.95	3.03	3.02	2.99	3.00	3.00	3.02	3.00	3.03	2.96	2.99	0.03
O[7]	12.19	12.44	11.87	11.45	11.66	11.96	11.58	11.59	11.56	11.78	11.67	11.41	11.58	11.71	0.27

[1] every 3rd analysis (numbered from rim to core) in the traverse on Fig. 2
[2] ave (average) and s.d. (standard deviation) from mean of 38 analyses
[3] negative values retained to yield meaningful average
[4] back-calculated
[5] normalized to Pb = 5
[6] 1−Cl
[7] framework O after subtraction of OH

TABLE 4. Analyses of mattheddleite grains using a celestite standard for S.

Oxide wt.%	1	2	3	4	5	6	7	8	9	ave	s.d.[1]
SO_3	6.88	7.05	7.59	7.55	7.33	7.45	7.06	6.71	7.22	7.20	0.17
P_2O_5	n.d.[2]	n.d.	n.d.	0.06	n.d.	n.d.	0.04	n.d.	n.d.	n.d.	0.05
SiO_2	7.95	8.14	7.29	7.53	7.73	7.73	8.00	8.26	7.93	7.84	0.12
PbO	83.32	83.24	81.52	83.02	83.22	82.51	83.52	83.01	82.61	82.89	0.80
Cl	1.29	1.01	1.94	1.85	1.74	1.70	1.21	0.87	1.45	1.45	0.53
H_2O[3]	0.34	0.33	0.32	0.31	0.32	0.32	0.33	0.32	0.32	0.31	0.13
Cl=O	−0.28	−0.24	−0.43	−0.41	−0.38	−0.38	−0.27	−0.19	−0.32	−0.32	–
Sum	99.54	99.54	98.23	99.73	100.06	99.33	99.89	99.98	99.00	99.37	0.99
Atoms[4]											
S	1.15	1.18	1.30	1.27	1.23	1.26	1.18	1.13	1.22	1.21	0.07
P	0.00	0.00	0.00	0.01	0.00	0.00	0.01	0.00	0.00	0.00	0.00
Si	1.77	1.82	1.66	1.69	1.72	1.74	1.78	1.85	1.78	1.76	0.06
Pb	5.00	5.00	5.00	5.00	5.00	5.00	5.00	5.00	5.00	5.00	0.24
O	11.51	11.67	11.71	11.70	11.62	11.76	11.61	11.57	11.72	11.65	0.45
Cl	0.49	0.38	0.75	0.70	0.66	0.65	0.46	0.33	0.55	0.55	0.05
OH[5]	0.51	0.62	0.25	0.30	0.34	0.35	0.54	0.67	0.45	0.45	0.05

[1] s.d. (standard deviation) of a single analysis: calculated from peak and background counts for standard and unknown
[2] not detected
[3] back-calculated
[4] normalized to Pb = 5
[5] 1−Cl

(Table 2). The peak shape for S-$K\alpha$ may change subtly for sulphates *vs*. sulphides, such that the peak shift program does not fully correct the result.

Step analyses every 2 μm were collected along the length of the zoned crystal labelled in Fig. 2. The wt.% Cl varies between 0.9 and 2.4 (equivalent to X_{Cl} = 0.3−0.9, Table 3; Fig. 4). Examination of the long section of some mattheddleite grains reveals a more complete history of Cl oscillations with three maxima (Fig. 3). These data are in general agreement with the ranges reported by Livingstone *et al.* (1987), who observed variation in Cl of 0.56−2.1 wt.% (X_{Cl} = 0.2−0.7), and Steele *et al.* (2000), who showed a zoned mattheddleite that varied from 1.0 wt.% Cl in the core up to 2.7 wt.% on the rim (X_{Cl} = 0.4−1.0).

The Pb mineral with low Z was also analysed (Table 5). It has an analytical total without CO_2 or H_2O of ~90% and molar Pb/S of ~4, suggesting that it is a leadhillite polymorph. Leadhillite and susannite were reported in the original description of the sample under study. The elements Na, P, Cl, V, As, Sr and Ba were also sought in this phase but are below their detection limits. This

TABLE 5. Analyses of other Pb minerals.

Wt.% # analyses	Leadhillite 8	Hydrocerussite 2
SiO_2	n.d.[1]	0.15
P_2O_5	n.d.	0.03
SO_3	7.30	0.80
PbO	83.66	87.74
CO_2[2]	8.25	11.53
H_2O[2]	1.69	2.36
Sum	100.90	102.61
Atoms	Pb = 4	Pb = 3
Si	n.d.	0.02
P	n.d.	0.00
S	0.98	0.08
Pb	4.00	3.00
O	2.00	8.27
H	2.00[3]	2.00[4]

[1] not detected
[2] back-calculated
[3] Pb/2
[4] 0.667*Pb

phase contains blades of a phase with higher BSE contrast (Fig. 1). It is beam-damaged after only a few seconds of electron beam exposure, even using a 5 μm scanning beam at 10 nA and 15 kV. The beam damage shows up as a bright spot in BSE contrast, indicating that it is rapidly degassed, thus increasing its average Z. The analyses indicate that the low-Z mineral in the host is a leadhillite polymorph and that the high-Z blades are hydrocerussite.

Discussion

IV site occupancy of mattheddleite

Mattheddleite was confirmed to have a fully occupied IV site, as concluded by Steele *et al.* (2000), based on structure-refinement studies. The cause of the apparent IV site deficiency observed in electron microprobe analyses of mattheddleite is here linked to problems of wavelength shift of the S-$K\alpha$ peak position, rather than errors in the absorption correction for S (Steele *et al.* 2000). Using galena as a standard reduces the IV site occupancy in mattheddleite by ~10% (Table 2), compared with nearly stoichiometric analyses of the same spots obtained with a celestite standard (Tables 3, 4).

The existence of OH-dominant mattheddleite

The analytical data in this study provide some evidence for variation between OH-dominant mattheddleite ($OH_{65}Cl_{34}$) and Cl-dominant mattheddleite (up to OH_6Cl_{94}) in a zoned crystal of mattheddleite. The Cl-rich mattheddleite forms distinct zones in mattheddleite (Figs 2, 3). The variation of Cl observed in this study is on such a small scale that a structure refinement of a crystal from this sample would represent an average across an inhomogeneous sample. Ferraris *et al.* (2006) obtained HRTEM measurements on a fluorapatite with minor substitution of Na, Si, S and Cl. They found nanoscale domains of apatite with different compositions inferred to be ellestadite and chlorapatite in the host fluorapatite. Such modulations may be the precursor of larger-scale exsolution, as reported by Stalder and Rozendaal (2002) between 'OH-pyromorphite' and fluorapatite. Mattheddleite could have similar domains, although the short time and temperature scale involved with formation of hydrothermal veins may not be conducive to even nanoscale exsolution. Additional mattheddleite samples should be studied from Leadhills to establish the physical and chemical properties of the possible new mineral, 'OH-mattheddleite', and to distinguish it from the Cl-dominant mineral mattheddleite.

Imbalance between Si and S in mattheddleite

In the original description of mattheddleite, the moles of Si were not matched by S (Livingstone *et al.*, 1987), unlike ellestadite group minerals (Rouse and Dunn, 1982). That result remains unchanged in this study. The cause of the imbalance of Si to S in average mattheddleite relative to the expected ideal formula, $Pb_5S_{1.5}Si_{1.5}O_{12}(Cl,OH)$, is difficult to resolve. Minor element substitution does not appear to play a role in perturbing the formula of mattheddleite. Steele *et al.* (2000) analysed Be, B, Mg, Al, P, Cr, Mn, As and V, but did not find measurable levels of those elements in mattheddleite. In this work, F, Ca, Mn, V, As, Sr, Y, Ba, La, Ce, Pr, Nd, Sm, Gd, Pb and Th were included in analyses but were not detected at levels above the detection limits (Table 1). Thus, only five of the 25 elements that were analysed in the two studies were detected in the same sample of mattheddleite. The average of 75 mattheddleite analyses in this study yields $Pb_5S_{1.2}Si_{1.8}O_{11.7}[Cl_{0.6}(OH)_{0.4}]$ normalized to five Pb cations. Possible explanations for the deficiency of −0.6 charges p.f.u. include substitution of: (1) REE^{3+} or Th^{4+} on the IX site, e.g. $Pb_{4.4}REE_{0.6}S_{1.2}Si_{1.8}O_{12}[Cl_{0.6}(OH)_{0.4}]$ or $Pb_{4.7}Th_{0.3}S_{1.2}Si_{1.8}O_{12}[Cl_{0.6}(OH)_{0.4}]$; (2) vacancy on the Cl site, $Pb_5S_{1.2}Si_{1.8}O_{12}$ $[Cl_{0.4}\square_{0.6}]$; (3) Cl on one of the O sites and OH on the R^- site, $Pb_5S_{1.2}Si_{1.8}[O_{11.4}Cl_{0.6}]OH$; (4) Pb^{4+} on the VI site $Pb^{4+}_{0.3}Pb^{2+}_{9.7}S_{1.2}Si_{1.8}O_{12}$ $[Cl_{0.6}(OH)_{0.4}]$; (5) oxygen vacancy, $Pb_5S_{1.2}Si_{1.8}$ $[O_{11.7}\square_{0.3}][Cl_{0.6}(OH)_{0.4}]$; or (6) a combination of the above explanations.

The absence of detectable Pb, Y, *REE* and Th indicates that that model 1 is untenable. Model 2 does not include enough Cl for most of the mattheddleite analyses. By shifting some of the Cl to the O site, model 3 requires an extra 0.6 OH p.f.u. if that site is filled, such that an accurate determination of H_2O would reveal that contribution. The mattheddleite sample of this study, however, is so heterogeneous that even a SIMS determination of H would represent some averaged value. Substitution of Cl for O and O for Cl + OH could be tested by structure refinements. The possibility of Pb^{4+} (model 4)

seems unlikely in the large cation sites of apatite. Model 5 is appealing as the substitution is well established in another apatite structure, finnemanite, $Pb_5[AsO_3\square]_3Cl$ (Effenberger and Pertlik, 1997), and the formula normalized to Pb = 5 remains correct. However, considering the lack of arsenate in mattheddleite, the structure may not tolerate an anion deficiency or a lower valence for S. Including the O from the OH, models 3 and 4 have 12.4 O p.f.u. and model 5 has 12.1 O p.f.u.

Direct analysis of oxygen in mattheddleite was undertaken in order to test among the viable models (Table 3). The 1σ uncertainty of an individual analysis of O is 0.11 wt.%, or 0.9 p.f.u. (Table 1). The average O in the zoned mattheddleite crystal is 12.1±0.2 p.f.u., where the uncertainty is calculated based on deviations from the mean of 38 analyses (Table 3). This result appears to confirm a deficiency in O, although the uncertainty in the average value is large enough to accommodate models 3 and 4 at the 1σ limit of the average O. The analysis of O suggests but does not definitively indicate the possibility of a 0.3 p.f.u. vacancy (□) substitution in the O site: $Pb_5S_{1.2}Si_{1.8}[O_{11.7}\square_{0.3}][Cl_{0.6}(OH)_{0.4}]$, or 0.3 Cl p.f.u. for O: $Pb_5S_{1.2}Si_{1.8}[O_{11.7}Cl_{0.3}][Cl_{0.3}(OH)_{0.4}\square_{0.3}]$. Minor substitution of O for OH was noted on the OH site in synthetic Pb-Ca fluorovanadinite (Dong and White, 2004*a*,*b*), where the additional O is not related to an oxygen deficiency, but this mechanism does not address a charge imbalance in mattheddleite with Si > S. Structure refinements should be undertaken on homogeneous crystals of matthedd-leite to evaluate the possibility of a 2.5% vacancy in the O site, 0.3 Cl + OH substituting for that O, or a 20–30% vacancy in the Cl site.

Mattheddleite reactions

The anglesite, cerussite, galena, hydrocerussite, lanarkite, lead, mattheddleite, minium, plattnerite, scotlandite, and the polymorphs leadhillite, macphersonite and susannite at Leadhills suggest the possibility of redox equilibria relating these minerals in the system Pb-Si-S-C-O-H. The minerals shannonite (Roberts *et al.*, 1995) and plumbotsumite (Keller and Dunn, 1982) may also be considered as possible additional phases. A reaction may be calculated with OH mattheddleite in f_{S_2}-f_{O_2} space and any one of the other Pb minerals, each of which would involve either quartz or a solution with dissolved aqueous silica. Reactions may also be balanced with stoichiometric mattheddleite, a Pb carbonate, a Pb sulphate and quartz or aqueous silica that involve only the fluid species H_2O and CO_2, as in the following equilibria:

$$\text{mattheddleite} + CO_2 + H_2O = \text{lanarkite} + \text{hydrocerussite} + \text{silica (xl, aq)} \quad (1)$$
$$6Pb_5(SiO_4)_{1.5}(SO_4)_{1.5}(OH) + H_2O + 8CO_2 = 9Pb_2OSO_4 + 4Pb_3(CO_3)_2(OH)_2 + 9SiO_2$$

$$\text{mattheddleite} + \text{hydrocerussite} + CO_2 + H_2O = \text{leadhillite} + \text{silica (xl, aq)} \quad (2)$$
$$6Pb_5(SiO_4)_{1.5}(SO_4)_{1.5}(OH) + 2Pb_3(CO_3)_2(OH)_2 + 4H_2O + 14CO_2 = 9Pb_4SO_4(CO_3)_2(OH)_2 + 9SiO_2$$

$$\text{mattheddleite} + CO_2 = \text{lanarkite} + \text{cerussite} + \text{silica (xl, aq)} \quad (3)$$
$$2Pb_5(SiO_4)_{1.5}(SO_4)_{1.5}(OH) + 4CO_2 = 3Pb_2OSO_4 + 4PbCO_3 + 3SiO_2 + H_2O$$

$$\text{hydrocerussite} + CO_2 = \text{cerussite} + H_2O \quad (4)$$
$$Pb_3(CO_3)_2(OH)_2 + CO_2 = 3PbCO_3 + H_2O$$

These and related reactions will behave similarly to the many equilibria that have been formulated for marbles in T–$X(H_2O)$–$X(CO_2)$ space. Equilibrium assemblages with mattheddleite or hydrocerussite will form at higher T or from an aqueous fluid with less CO_2 than lanarkite-hydrocerussite-quartz, leadhillite-quartz, and cerussite. Reactions 1 and 3 each bound the stability of mattheddleite, and their intersection yields an invariant point through which reaction 4 also passes. If reactions 1 and 2 are both stable, reaction 1 must occur at lower T than reaction 2. The formation of mattheddleite later than leadhillite-quartz at Leadhills is counterintuitive considering reaction 2, and it suggests that the fluid evolved to a more CO_2-depleted composition, or that a hotter fluid was introduced in the later stages of hydrothermal activity. The Leadhills deposit may have formed from a boiling fluid in the presence of a gaseous phase rich in CO_2 and a liquid rich in H_2O. If any of the reactions 1–4 intersect the CO_2–H_2O solvus, it becomes invariant in T-X space in the presence of two fluid species. If so, and if only very minor amounts of additional fluid species such as SO_2, NaCl, HCl, or SO_3 are present, these reactions will serve as useful thermometers at a given fluid pressure.

Abdul-Samad *et al.* (1982) measured the free energy of lanarkite with solution techniques at

STP and calculated ionic equilibria among anglesite, cerussite, galena, hydrocerussite, lanarkite and leadhillite. That approach could be extended to include alamosite, macphersonite, mattheddleite, plumbotsumite, scotlandite, shannonite and susannite once thermodynamic data are available for those phases. Abdul-Samad *et al.* (1982) showed that lanarkite is stable only at a very low activity of H_2CO_3, which explains its rarity even at Leadhills. Livingstone (1993) also discussed reactions involving leadhillite polymorphs. The locus of the reactions relating the phases in Pb-Si-S-C-O-H could then be computed at selected *P-T-X* conditions applicable to Leadhills, Tsumeb, and other lead deposits, similar to thermodynamic studies that have been undertaken on telluride (Afifi *et al.*, 1988*a*,*b*) and selenide ore deposits (Simon and Essene, 1996; Simon *et al.*, 1997).

Thermal stability of mattheddleite

Derriche and Perrot (1976) showed that Pb_2SO_4O (lanarkite), $Pb_3SO_4O_2$ and $Pb_5SO_4O_4$ are stable on the join $PbO-PbSO_4$ up to their melting points at 900–950ºC. Stoichiometric OH-mattheddleite should therefore dehydrate to $Pb_5SO_4O_4$, $Pb_3SO_4O_2$ and SiO_2 via a reaction such as:

mattheddleite =
$Pb_3SO_4O_2 + Pb_5SO_4O_4$ + quartz + fluid (5)
$4Pb_5(SiO_4)_{1.5}(SO_4)_{1.5}(OH) =$
$5Pb_3SO_4O_2 + Pb_5SO_4O_4 + 6SiO_2 + 2H_2O$

One could balance a related reaction for non-stoichiometric mattheddleite once its formula is better established. Given the relatively low OH content of stoichiometric mattheddleite, its stability may extend to high temperatures (600–800ºC?) at high H_2O pressure (above a few kbar?). The phases $Pb_3SO_4O_2$ and $Pb_5SO_4O_4$ should be sought in late-stage associations at Leadhills, where they may be found in assemblages that grew at low H_2O and CO_2 pressure.

Paragenetic sequence of lead minerals at Leadhills

Temple (1956), Gillanders (1981) and Abdul-Samad *et al.* (1982) discussed the paragenetic sequence of Pb minerals at Leadhills, which is: galena → anglesite → cerussite → leadhillite → lanarkite and cerussite → hydrocerussite. Those sequences may be linked with a series of phase equilibria. Livingstone *et al.* (1987) reported the assemblage mattheddleite-quartz-cerussite, which would buffer the composition of the fluid if formed at equilibrium. Paar *et al.* (1984*a*) inferred that scotlandite, lanarkite and susannite were the latest-stage minerals at Leadhills. The overgrowths of mattheddleite on leadhillite (and/or susannite) and hydrocerussite (Fig. 1) also suggest that mattheddleite is a later part of the paragenesis. Dissolution textures were observed on leadhillite crystals from Caldbeck Fells (Cooper and Stanley, 1990). The process of dissolution on earlier-formed Pb minerals may provide a supply of lead for the later paragenetic sequence involving Pb minerals. Reactions 1–4 apply to later stages of the paragenetic sequence. The extended paragenetic sequence at Leadhills is galena → anglesite → cerussite → leadhillite-susannite-hydrocerussite → mattheddleite-lanarkite-scotlandite, where lanarkite and scotlandite are also late but the parageneses of which are still not well established relative to mattheddleite or each other. The role of plattnerite at Leadhills is unclear, and whether minium or native lead occur as Leadhills minerals remains to be established. Consideration of reactions among the Pb minerals collectively indicates that their relative stability depends on fluid composition for a given *P-T*. In many hydrothermal environments, however, equilibrium processes are overstepped with crystallization from a supersaturated fluid as well as nucleation and growth of metastable phases at low temperatures (<200ºC). The role of metastability during crystallization of the hydrothermal assemblages at Leadhills (Livingstone, 1993) is in need of further evaluation. Equilibrium assemblages and reactions would provide only an approximate guide to the understanding of disequilibrium systems.

Cl zoning in mattheddleite

The remarkable oscillatory zoning of Cl in mattheddleite must be related to salinity changes in the hydrothermal fluid. One may posit an exchange reaction between OH-Cl mattheddleite and aqueous fluid:

OH-dominant mattheddleite + HCl =
Cl-dominant mattheddleite + H_2O (6)
$Pb_5(SiO_4)_{1.5}(SO_4)_{1.5}(OH) + H^+ + Cl^- =$
$Pb_5(SiO_4)_{1.5}(SO_4)_{1.5}Cl + H_2O$

The Cl/OH content of mattheddleite thus is controlled by pH as well as pCl or chlorinity and *T*. The amount of OH in mattheddleite will also depend on whether the vacancy substitutes in the

structure or not. Three cycles of high Cl are evident in the analytical traverse (Fig. 3), where the Cl peaks indicate a physiochemical change in the fluid. The reports of vanadinite, mimetite and pyromorphite (lead chloride vanadate, arsenate and phosphate, respectively) in veins at Leadhills (Brown, 1919; Temple, 1956; Gillanders, 1981; Livingstone, 1994b) indicate that late-stage fluids were highly oxidized and enriched in Cl. The hydrothermal fluid at Leadhills probably varied in salinity as it migrated and evolved as a result of crystallization, dissolution and/or replacement of earlier crystallized solids. The Cl variations observed in mattheddleite may result from degassing during boiling and/or mixing with a more saline fluid.

Recommendations

Analysis of sulphate-bearing minerals

The sulphate in apatite or indeed that in any other sulphate should never be analysed using sulphide standards with wavelength dispersive methods on an electron microprobe. Livingstone and Sarp (1984) reported analyses of Leadhills macphersonite including S with a galena standard at unstated conditions with an electron microprobe. The S is less than expected by ~10% of the amount present, which probably resulted from the use of the galena standard. Macphersonite from Saint-Prix, France, was analysed by gravimetric means, and there the S is much closer to stoichiometric levels. Sarp and Perroud (1991) used chalcopyrite in the analysis of S in camerolaite. Liu and Comodi (1993) employed sphalerite as a standard for analysis of S in apatite, obtaining 0.02–1.64 wt.% SO_3 in 24 samples from carbonatites and alkaline igneous rocks. Livingstone (1994*a*) obtained 0.09–0.23 wt.% SO_3 in plumbian apatite with galena as a standard for S. Golebiowska *et al.* (2002) used a pyrite standard for S in the analysis of a sulphate-bearing mimetite. The S standards were not specified in several studies involving WDS analyses of sulphatoan scapolite (Griffin *et al.*, 1979; Okrusch *et al.*, 1979; Austrheim and Griffin, 1985), alunite (Deyell and Dipple, 2005; Deyell *et al.*, 2005), and scotlandite (Sarp and Burri, 1984). The scotlandite analysis of Sarp and Burri (1984) has a low analytical total and 22% deficiency of S compared to Pb, suggesting a large systematic error in the S, which implies that a sulphide standard was used in its analysis. Scotlandite is a sulphite and not a sulphate, and the possibility of a shift in the position of the S-$K\alpha$ peak between sulphites and sulphates remains to be evaluated. Scotlandite may show solid solution towards alamosite via the exchange Si-S, it may contain Ba or Sr, and substitutions such as *REE*·Al-Pb·S should be evaluated. A systematic error of negative 10–20% OAP is anticipated whenever sulphide standards are used for sulphates with WDS analysis.

Sulphate standards were employed in WDS analyses of S in apatite group minerals (Rouse and Dunn, 1982; Shiga and Urashima, 1987), scotlandite (Paar *et al.*, 1984*a*), scapolite (Coolen, 1980; Moecher and Essene, 1990, 1991), baryte and celestite (Boundy *et al.*, 2002), and complex hydrous sulphate minerals (Keller *et al.*, 1979; Paar *et al.*, 1984*b*; Jackson, 1990; Li *et al.*, 1992; Peacor *et al.*, 1999*a*,*b*; Rouse *et al.*, 2001; Drouet and Navrotsky, 2003; Pe-Piper and Dolansky, 2005). Those analyses are not anticipated to have serious errors due to systematic shifts in the position of the S peak. Selecting the proper standard for a phase with S in an unknown bonding type should necessitate wavelength scans on the unknown *vs*. selected sulphate and sulphide standards to decide upon the best standard for that phase.

Significance of sulphate substitution in apatite-group minerals

Studies of rock-forming apatite should include routine analysis of S with a sulphate standard. Core *et al.* (2006) used the sulphate substitution of apatite to evaluate the oxidation state and degassing history during crystallization of granitic rocks. They extracted the thermodynamic properties of hydroxylellestadite from experiments and showed that its substitution in apatite, buffered in the presence of anhydrite-quartz and clinopyroxene-quartz, is favoured at more oxidizing conditions. Such applications will continue to be limited, however, until S is routinely analysed in rock-forming apatite from a wide variety of associations. Sulphur may be present in any apatite with detectable Na or Si, and therefore it should be included in the electron microprobe analytical procedure.

Future geochemical studies at Leadhills

Growth of zoned mattheddleite appears to be a faithful recorder of changes in the composition of the hydrothermal fluid. Fluid-inclusion studies in the lead minerals and/or cogenetic quartz may be

useful in unravelling the fluid chemistry, and whether the hydrothermal fluid(s) underwent one or more stages of boiling or degassing as it evolved. Measurement of the brine and CO_2 content in fluid inclusions would be of considerable interest in understanding the salinity and alkalinity of the ore fluid, and its changes during the later stages of hydrothermal activity that produced the lead mineral assemblages at Leadhills.

Acknowledgements

This work was supported by NSF grants EAR 96-28196, 99-11352 and 02-30098, and the W.C. Kelly Collegiate Professorship to EJE. Roland C. Rouse and Ian M. Steele are thanked for their reviews and suggestions which improved the manuscript.

References

Abdul-Samad, F.A., Thomas, J.H., Williams, P.A. and Symes, R.F. (1982) Chemistry of formation of lanarkite, Pb_2OSO_4. *Mineralogical Magazine*, **46**, 499–501.

Afifi, A.M. and Essene, E.J. (1988) Minfile: a microcomputer program for storage and manipulation of chemical data on minerals. *American Mineralogist*, **73**, 446–448.

Afifi, A.M., Kelly, W.C. and Essene, E.J. (1988*a*) The stability and phase relations of tellurides. Part I. Thermochemical data and calculated equilibria. *Economic Geology*, **83**, 377–394.

Afifi, A.M., Kelly, W.C. and Essene, E.J. (1988*b*) The stability and phase relations of tellurides. Part II. Applications to telluride-bearing ore deposits. *Economic Geology*, **83**, 394–404.

Austrheim, H. and Griffin, W.L. (1985) Shear deformation and eclogite formation within granulite-facies anorthosites of the Bergen Arcs, Western Norway. *Chemical Geology*, **50**, 267–281.

Barth, A.P. and Dorais, M.J. (2000) Magmatic anhydrite in granitic rocks: first occurrence and potential petrologic consequences. *American Mineralogist*, **85**, 430–435.

Boucher, M.L. and Peacor, D.R. (1968) The crystal structure of alamosite, $PbSiO_3$. *Zeitschrift für Kristallographie, Kristallgeometrie, Kristallphysik, Kristallchemie*, **127**, 99–111.

Boundy, T.M., Donohue, C.L., Essene, E.J., Mezger, K. and Austrheim, H. (2002) Discovery of eclogite-facies carbonate rocks from the Lindås Nappe, Western Norway. *Journal of Metamorphic Geology*, **20**, 649–667.

Brown, R. (1919) The mines and minerals of Leadhills. *Transactions and Journal of Proceedings of the Dumfriesshire and Galloway Natural History & Antiquarian Society*, **6**, 124–137.

Carroll, M.R. and Rutherford, M.J. (1988) Sulfur speciation in hydrous experimental glasses of varying oxidation state: results from measured wavelength shifts of sulfur X-rays. *American Mineralogist*, **73**, 845–849.

Cavarretta, G., Mottana, A. and Tecce, F. (1981) Cesanite, $Ca_2Na_3[(OH)(SO_4)_3]$, a sulphate isotypic to apatite from the Cesano geothermal field (Latium, Italy). *Mineralogical Magazine*, **44**, 269–273.

Chakhmouradian, A.R. and Medici, L. (2006) Clinohydroxylapatite: a new apatite-group mineral from northwestern Ontario (Canada), and new data on the extent of Na-S substitution in natural apatites. *European Journal of Mineralogy*, **18**, 105–112.

Connolly, J.W.D. and Haughton, D.R. (1972) The valence of sulfur in glass of basaltic composition formed under conditions of low oxidation potential. *American Mineralogist*, **57**, 1515–1519.

Coolen, J.J.M.M.M. (1980) Chemical petrology of the Furua granulite complex, southern Tanzania. *GUA Papers of Geology*, **1**, 13, 258 pp.

Cooper, M.P. and Stanley, C.J. (1990) Minerals from the English Lake District, Caldbeck Fells. *Natural History Museum Publications*, London, 160 pp.

Core, D.P., Essene, E.J., Kesler, S.E. and Luhr, J.F. (2006) Thermodynamic properties of sulfatian apatite: constraints on the behavior of sulfur in calc-alkaline igneous rocks. *American Mineralogist*, (submitted).

Derriche, Z. and Perrot, P. (1976) Thermodynamic study of the solid and liquid phases in the lead(II) oxide-lead(II) sulfate system. *Revue de Chimie Minerale*, 1**3**, 310–323.

Deyell, C.L. and Dipple, G.M. (2005) Equilibrium mineral-fluid calculations and their application to the solid solution between alunite and natroalunite in the El Indio-Pascua belt of Chile and Argentina. *Chemical Geology*, **215**, 219–234.

Deyell, C.L., Rye, R.O., Landis, G.P. and Bissig, T. (2005) Alunite and the role of magmatic fluids in the Tambo high-sulfidation deposit, El Indio-Pascua belt, Chile. *Chemical Geology*, **215**, 185–218.

Dong, Z.L. and White, T.J. (2004*a*) Calcium-lead fluoro-vanadinite apatites. I. Disequilibrium structures. *Acta Crystallographica*, **B60**, 138–145.

Dong, Z.L. and White, T.J. (2004*b*) Calcium-lead fluoro-vanadinite apatites. II. Equilibrium structures. *Acta Crystallographica*, **B60**, 146–154.

Drouet, C. and Navrotsky, A. (2003) Synthesis, characterization, and thermochemistry of K-Na-H_3O jarosites. *Geochimica et Cosmochimica Acta*, **67**, 2063–2076.

Effenberger, H. and Pertlik, F. (1997) Die Kristallstruktur des Finnemanits, $Pb_5Cl(AsO_3)_3$, mit einem Vergleich zum Strukturtyp des Chlorapatits, $Ca_5Cl(PO_4)_3$. *Tschermaks Mineralogische und Petrographische Mitteilungen*, **26**, 95–107.

Essene, E.J. (1989) The current status of thermobarometry in metamorphic rocks. Pp. 1–44 in: *Evolution of Metamorphic Belts* (S.R. Daly, R. Cliff and B.W.D. Yardley, editors). Special Publication, **43**, Geological Society, London.

Ferraris, C., White, T.J., Plévert, J. and Wegner, R. (2006) Nanometric modulation in apatite. *Physics and Chemistry of Minerals*, (submitted).

Gillanders, R.J. (1981) Famous mineral localities: the Leadhills-Wanlockhead district, Scotland. *Mineralogical Record*, **12**, 235–250.

Gołębiowska, B., Pieczka, A. and Franus, W. (2002) Ca-bearing phosphatian mimetite from Rędziny, Lower Silesia, Poland. *Neues Jahrbuch für Mineralogie Monatshefte*, 31–41.

Griffin, W.L., Carswell, D.A. and Nixon, P.H. (1979) Lower-crustal granulites and eclogites from Lesotho, Southern Africa. Pp. 59–86 in: *The Mantle Sample: Inclusions in Kimberlites and Other Volcanics* (F.R. Boyd and H.O.A. Meyer, editors). Proceedings of the Second International Kimberlite Conference, AGU, Washington DC.

Harada, K., Nagashima, K., Nakao, K. and Kato, A. (1971) Hydroxylellestadite, a new apatite from Chichibu Mine, Saitama prefecture, Japan. *American Mineralogist*, **56**, 1507–1518.

Hughes, J.M. and Drexler, J.W. (1991) Cation substitution in the apatite tetrahedral site: crystal structures of type hydroxylellestadite and type fermorite. *Neues Jahrbuch für Mineralogie Monatshefte*, 327–336.

Jackson, B. (1990) Queitite, a first Scottish occurrence. *Scottish Journal of Geology*, **26**, 57–58.

Keller, P. and Dunn, P.J. (1982) Plumbotsumite, $Pb_5(OH)_{10}Si_4O_8$, a new lead silicate from Tsumeb, Namibia. *Chemie der Erde*, **41**, 1–6.

Keller, P., Dunn, P.J. and Hess, H. (1979) Queitite, $Pb_4Zn_2SO_4(SiO_4)_4Si_2O_7$, ein neues Mineral aus Tsumeb, Südwesafrika. *Neues Jahrbuch für Mineralogie Monatshefte*, 203–209.

Li, G., Peacor, D.R., Essene, E.J., Brosnahan, D.R. & Beane, R.E. (1992) Walthierite and huangite, two new minerals of the alunite group, from El Indio Mine, Chile. *American Mineralogist*, **77,** 1275–1284.

Liu, Y. and Comodi, P. (1993) Some aspects of the crystal-chemistry of apatites. *Mineralogical Magazine*, **57**, 709–719.

Livingstone, A. (1993) Origin of the leadhillite polymorphs. *Journal of the Russell Society*, **5**, 11–13.

Livingstone, A. (1994*a*) An apatite high in lead from Wanlockhead, Strathclyde Region, Scotland. *Mineralogical Magazine*, **58**, 159–163.

Livingstone, A. (1994*b*) Analyses of calcian phosphatian vanadinite, and apatite high in lead, from Wanlockhead, Scotland. *Journal of the Russell Society*, **5**, 124–126.

Livingstone, A. (2002) *Minerals of Scotland*. National Museums of Scotland, Edinburgh, 212 pp.

Livingstone, A. and Russell, J.D. (1985) X-ray powder data for susannite and its distinction from leadhillite. *Mineralogical Magazine*, **49**, 759–761.

Livingstone, A. and Sarp, H. (1984) Macphersonite, a new mineral from Leadhills, Scotland, and Saint-Prix, France: a polymorph of leadhillite and susannite. *Mineralogical Magazine*, **48**, 277–282.

Livingstone, A., Ryback, G., Fejer, E.E. and Stanley, C.J. (1987) Mattheddleite, a new mineral of the apatite group from Leadhills, Strathclyde region. *Scottish Journal of Geology*, **23**, 1–8.

Lovering, J.F. and Widdowson, J.R. (1968*a*) Electron-microprobe analysis of anandite. *Mineralogical Magazine*, **36**, 871–874.

Lovering, J.F. & Widdowson, J.R. (1968*b*) Electron microprobe determination of sulphur coordination in minerals. *Lithos*, **1**, 264–267.

Matthews, S.J., Moncrieff, D.H.S. and Carroll, M.R. (1999) Empirical calibration of the sulphur valence oxygen barometer from natural and experimental glasses: method and applications. *Mineralogical Magazine*, **63**, 421–431.

McConnell, D. (1937) The substitution of SiO_4- and SO_4-groups for PO_4-groups in the apatite structure; ellestadite, the end member. *American Mineralogist*, **22**, 977–986.

Moecher, D.P. and Essene, E.J. (1990) Phase equilibria for calcic scapolite, and implications of variable Al-Si disorder on P-T, T-X_{CO2}, and a-X relations. *Journal of Petrology*, **31**, 997–1024.

Moecher, D.P. and Essene, E.J. (1991) Calculation of CO_2 activities from scapolite equilibria: constraints on the presence of a fluid phase during high grade metamorphism. *Contributions to Mineralogy and Petrology*, **108**, 219–240.

Okrusch, M., Schröder, B. and Schnütgen, A. (1979) Granulite facies metabasite ejecta in the Laacher See area, Eifel, West Germany. *Lithos*, **12**, 251–270.

Paar, W.H., Braithwaite, R.S.W., Chen, T.T. and Keller, P. (1984*a*) A new mineral, scotlandite ($PbSO_3$) from Leadhills, Scotland: the first naturally occurring sulphite. *Mineralogical Magazine*, **48**, 283–288.

Paar, W.H., Mereiter, K., Braithwaite, R.S.W., Keller, P. and Dunn, P.J. (1984*b*) Chenite, $Pb_4Cu(SO_4)_2(OH)_6$, a new mineral from Leadhills, Scotland. *Mineralogical Magazine*, **50**, 129–135.

Peacor, D.R., Rouse, R.C., Coskren, T.D. and Essene, E.J. (1999*a*) Destinezite ("diadochite"), $Fe_2(PO_4)(SO_4)\cdot 6H_2O$: its crystal structure and role

as a soil component at Alum Cave Bluff, Tennessee. *Clays and Clay Minerals*, **47**, 1–11.

Peacor, D.R., Rouse, R.C., Essene, E.J. and Lauf, R. (1999*b*) Coskrenite, a new Ce oxalate mineral from Alum Cave Bluff, Tennessee: characterization and crystal structure. *The Canadian Mineralogist*, **37**, 1453–1462.

Peng, G., Luhr, J.F. and McGee, J.J. (1997) Factors controlling sulfur concentrations in volcanic apatite. *American Mineralogist*, **82**, 1210–1224.

Pe-Piper, G. and Dolansky, L.M. (2005) Early diagenetic origin of Al phosphate-sulfate minerals (woodhouseite and crandallite series) in terrestrial sandstones, Nova Scotia, Canada. *American Mineralogist*, **90**, 1434–1441.

Piotrowski, A., Kahlenberg, V., Fischer, R.X. and Parise, J.B. (2002) The crystal structures of cesanite and its synthetic analog – a comparison. *American Mineralogist*, **87**, 715–720.

Roberts, A.C., Stirling, J.A.R., Carpenter, G.J.C., Criddle, A.J., Jones, G.C., Birkett, T.C. and Birch, W.D. (1995) Shannonite, Pb_2OCO_3, a new mineral from the Grand Reef Mine, Graham County, Arizona, USA. *Mineralogical Magazine*, **59**, 305–310.

Rouse, R.C. and Dunn, P.J. (1982) A contribution to the crystal chemistry of ellestadite and the silicate sulfate apatites. *American Mineralogist*, **67**, 90–96.

Rouse, R.C., Peacor, D.R., Coskren, T.D., Essene, E.J. and Lauf, R.J. (2001) The new minerals levinsonite-(Y) [$(Y,Nd,Ce)Al(SO_4)_2C_2O_4{\cdot}12H_2O$] and zugshunstite-(Ce) [$(Ce,Nd,La)Al(SO_4)_2C_2O_4{\cdot}12H_2O$]: coexisting phases with different structures exhibiting strong differentiation of LREE and HREE. *Geochimica et Cosmochimica Acta*, **65**, 1101–1115.

Sarp, H. and Burri, G. (1984) Seconde occurrence du nouveau mineral scotlandite $PbSO_3$. *Schweizerische Mineralogische und Petrographische Mitteilungen*, **64**, 317–321.

Sarp, H. and Perroud, P. (1991) Camerolaite, $Cu_4Al_2[HSbO_4,SO_4](OH)_{10}(CO_3).2H_2O$, a new mineral from Cap Garonne mine, Var, France. *Neues Jahrbuch für Mineralogie Monatshefte*, 481–486.

Seeliger, E. and Berdesinski, W. (1956) Zur Genese des Caracolit in der Lagerstaette "Stein V". *Neues Jahrbuch für Mineralogie Monatshefte*, 25–32.

Shiga, Y. and Urashima, Y. (1987) A sodian sulfatian fluorapatite from an epithermal calcite-quartz vein of the Kushikino Mine, Kagoshima Prefecture, Japan. *The Canadian Mineralogist*, **25**, 673–681.

Simon, G. and Essene, E.J. (1996) Phase relations among selenides, sulfides, tellurides and oxides. I. Thermodynamic data and calculated equilibria. *Economic Geology*, **91**, 1183–1208.

Simon, G., Kesler, S.E. and Essene, E.J. (1997) Phase relations among selenides, sulfides, tellurides and oxides. II. Applications to selenide deposits. *Economic Geology*, **92**, 468–484.

Stalder, M. and Rozendaal, A. (2002) Graftonite in phosphatic iron formations associated with the mid-Proterozoic Gamsberg Zn-Pb deposit, Namaqua Province, South Africa. *Mineralogical Magazine*, **66**, 915–927.

Steele, I.M., Pluth, J.J. and Livingstone, A. (2000) Crystal structure of mattheddleite: a Pb, S, Si phase with the apatite structure. *Mineralogical Magazine*, **64**, 915–921.

Stormer, J.C., Pierson, M.L. and Tacker, R.C. (1993) Variation of F and Cl X-ray intensity due to anisotropic diffusion in apatite during electron microprobe analysis. *American Mineralogist*, **78**, 641–648.

Streck, M.J. and Dilles, J.H. (1998) Sulfur evolution of oxidized arc magmas as recorded in apatite from a porphyry copper batholith. *Geology*, **26**, 523–526.

Temple, A.K. (1956) The Leadhills-Wanlockhead lead and zinc deposit. *Transactions of the Royal Society of Edinburgh*, **63**, 96–113.

Wallace, P. and Carmichael, I.S.E. (1994) S speciation in submarine basaltic glasses as determined by measurements of S Kα X-ray wavelength shift. *American Mineralogist*, **79**, 161–167.

[*Manuscript received 10 January 2006: revised 13 June 2006*]